Interference errors in infrared remote sounding of the atmosphere

R. Sussmann, T. Borsdorff

Atmos. Chem. Phys. Discuss., 6, 13027–13073, 2006
www.atmos-chem-phys-discuss.net/6/13027/2006/

Atmospheric Chemistry and Physics Discussions

Interference errors in infrared remote sounding of the atmosphere

R. Sussmann and T. Borsdorff

IMK-IFU, Forschungszentrum Karlsruhe, Garmisch-Partenkirchen, Germany

Received: 13 November 2006 – Accepted: 6 December 2006 – Published: 12 December 2006

Correspondence to: R. Sussmann (ralf.sussmann@imk.fzk.de)

Abstract

More and more profiles of atmospheric state parameters are being retrieved from remote soundings in the infrared spectral domain. Classical error analysis, which was originally applied to microwave sounding systems, distinguishes between "smoothing errors," "forward model errors," "forward model parameter errors," and "retrieval noise errors". We show that for infrared soundings "interference errors", which have not been treated up to now, can be significant. Interference errors originate from "interfering species" that introduce signatures into the spectral measurement which overlap with the spectral features used for retrieval of the target species. This is a frequent situation in infrared atmospheric spectra where the vibration-rotation bands of different species often overlap; it is not the case in the microwave region. This paper presents a full theoretical formulation of interference errors. It requires a generalized state vector including profile entries for all interfering species. This leads to a generalized averaging kernel matrix made up of classical averaging kernels plus here defined "interference kernels". The latter are used together with climatological covariances for the profiles of the interfering species in order to quantify the interference errors. To illustrate the methods we apply them to a real sounding and show that interference errors have a significant impact on standard CO profile retrievals from ground-based mid-infrared solar absorption spectra. We also demonstrate how to minimize overall error, which is a trade-off between minimizing interference errors and the smoothing error. The approach used in this paper can be applied to soundings of all infrared-active atmospheric species, which includes more than two dozen different gases relevant to climate and ozone. And this holds for all kind of infrared remote sounding systems, i.e., retrievals from ground-based, balloon-borne, airborne, or satellite spectroradiometers.

ACPD

6, 13027–13073, 2006

1 Introduction

During the last decade, more and more, infrared remote sounding measurements have been used to obtain profiles of atmospheric composition and temperature from ground or space. Infrared profiling techniques complement the older microwave profilers in many ways, e.g., with respect to the altitude range attainable, and the atmospheric trace species under consideration. The theoretical framework for retrieval of profiles from spectral measurements via optimal estimation (OE) was developed three decades ago (Rodgers, 1976) and has been applied solely to microwave soundings for a long time. In addition, a concept for error analysis was formulated (Rodgers, 1990) to distinguish between four different classes of errors, i.e., "smoothing errors," "forward model errors," "forward model parameter errors" and "retrieval noise errors". In the last few years, this classical error analysis has also been applied to infrared retrievals. However, in infrared, a very frequently encountered problem in retrieving the "target quantity" is due to "interfering species." This occurs because the vibration-rotation bands of different species often overlap in the infrared atmospheric spectrum. Overlapping of this kind does not occur in the microwave region. Keeping in mind that the wings of (infrared) spectral lines always expand asymptotically towards plus-minus infinity in the frequency domain, it becomes clear that individual spectral lines used for the profile retrieval of an atmospheric target species, in principle, always overlap with neighboring spectral lines of other interfering species. This necessitates the simultaneous retrieval of the interfering species in the infrared and leads to a new class of errors, called "interference errors". Interference errors originate from the fact that the profile retrieval of an interfering species is usually not perfect (i.e., the averaging kernel matrix is not identical to the unit matrix, as a result of any type of regularization); this causes spectral residuals (measured minus simulated) around the spectral signature of the interfering species. In consequence, the (simultaneous) profile retrieval of the target species tends to compensate for this, meaning that an artifact is introduced into the retrieved target profile. While an experienced spectroscopist might be able to "see" potential

ACPD
6, 13027–13073, 2006

interference effects by visual inspection of the spectral features within a micro-window as a result of his understanding of all retrieval settings, this intuitive approach risks missing "hidden" interference effects and/or underestimating them quantitatively.

In addition to the described effect from the retrieval of interfering species we will include in "interference errors" all errors in a retrieved atmospheric target profile which originate from the regularization of the retrieval of any additional vector-type physical quantity. For example, temperature profiles retrieved at the same time as the target species, which may be used in order to minimize errors from insufficient knowledge of the true temperature profile at the time of observation.

More specifically, we want to add what our concept of interference errors does not currently mean. It does not have to do with any possible error in the forward modeling, i.e., either with errors in the forward model parameters, such as errors in the spectroscopic parameters of interfering species (e.g., an erroneous pressure broadening parameter), or with errors in the forward model itself like errors in line shape modeling (e.g., a non-Voigt type line shape of an interfering water vapor line, modeled by a Voigt-type forward model). Both kinds of errors will also lead to residuals in the retrieval of the interfering species, and, thereby introduce errors to the retrieval of the target species. For this reason, these effects have also sometimes been referred to as "interference errors". However, these two error classes clearly can be attributed to and treated as "forward model parameter errors" (above example of errors in spectroscopic parameters) and to "forward model errors" (above example of errors in line shape modeling). These are two error classes which had previously been named this way and formally been treated by Rodgers (1990, 2000). Interference errors are also different but in a sense related to "smoothing errors" (Rodgers, 1990, 2000), since for their quantification the regularization matrix of the retrieval as well as an estimate of true covariance of the interfering species has to be known (in case of smoothing errors: regularization matrix and covariance of the target species).

Up to now, interference errors have not been treated in a rigorous and quantitative way, although a theoretical formulation for treatment of all possible further classes of

ACPD
6, 13027–13073, 2006

EGU

errors (i.e., smoothing errors, forward model parameter errors, forward model errors, and errors from measurement noise) has previously been described in the literature (Rodgers, 1990, 2000; Connor et al., 1995). Therefore, these classes of errors will not be discussed in this paper. Rather, we will discuss interference errors quantitatively for the first time, and show their significance in terms of their magnitude relative to smoothing errors. We dedicate this paper to the treatment of interference errors since they can often become comparable to or sometimes even larger than smoothing errors in quantitative terms.

This paper starts with definitions and a recap of the classical error analysis according to Rodgers (Sect. 2). Section 3 is the central part of this paper and gives a general theoretical formulation to quantify interference errors. This general formulation can be used to optimize micro-windows, retrieval settings, and regularization strategies. In Sect. 4 our general method is illustrated by applying it to a real infrared sounding. As an example, the retrieval of CO profiles is illustrated for a test ensemble of ground-based solar spectra recorded with the high resolution Fourier transform spectrometer at the NDACC (Network for the Detection of Atmospheric Composition Change) Primary Station Zugspitze, Germany (see, e.g., Sussmann and Schäfer, 1997; Sussmann et al., 2005a, b). The interference errors found in the CO profiles from ozone, water vapor and all other interfering species have been quantified in detail. Section 5 presents two case studies showing how the error analysis can be used to test ways of reducing interference errors, e.g., via changing micro-window sets or optimizing regularization constraints for the retrieval of the interfering species. Finally, Sect. 6 presents some of the conclusions which can be drawn from this.

2 Definitions and classical error analysis

Our formulation of interference errors in Sect. 3 is an extension of Roger's (1990) formulation of error analysis which has been supplemented by Rodgers (2000). Therefore, we first briefly repeat the Rodgers (2000) formulation and the definitions used.

ACPD
6, 13027–13073, 2006

EGU

According to Rodgers (2000, Eq. 3.16) the retrieved target profile $\hat{\boldsymbol{x}}$ is related to the true target profile $\boldsymbol{x}$ via the relation

$$\begin{aligned}\hat{\boldsymbol{x}} - \boldsymbol{x} \quad = \quad & (\mathbf{A} - \mathbf{I})(\boldsymbol{x} - \boldsymbol{x}_a) \quad \ldots \text{ smoothing error} \\ & + \mathbf{G}_y \mathbf{K}_b (\boldsymbol{b} - \hat{\boldsymbol{b}}) \quad \ldots \text{ model parameter error} \\ & + \mathbf{G}_y \Delta \boldsymbol{f}(\boldsymbol{x}, \boldsymbol{b}, \boldsymbol{b}') \quad \ldots \text{ forward model error} \\ & + \mathbf{G}_y \boldsymbol{\varepsilon} \quad \ldots \text{ retrieval noise}\end{aligned} \tag{1}$$

where $\mathbf{A} = \partial \hat{\boldsymbol{x}} / \partial \boldsymbol{x}$, $\mathbf{G}_y = \partial \hat{\boldsymbol{x}} / \partial \boldsymbol{y}$, $\mathbf{K}_b = \partial \boldsymbol{F} / \partial \boldsymbol{b}$, and $\boldsymbol{x}_a$ is the a priori profile. The forward model parameters (which are not retrieved) are $\boldsymbol{b}$, and $\hat{\boldsymbol{b}}$ is our best estimate of the forward model parameters, as distinct from the true value $\boldsymbol{b}$. The forward function $\boldsymbol{f}$ describes the true physical relation between the measurement vector $\boldsymbol{y}$ and $\boldsymbol{x}$

$$\boldsymbol{y} = \boldsymbol{f}(\boldsymbol{x}, \boldsymbol{b}, \boldsymbol{b}') + \boldsymbol{\varepsilon} \tag{2}$$

Measurement noise is described by the error term $\boldsymbol{\varepsilon}$. The forward model $\boldsymbol{F}$ is related to $\boldsymbol{f}$ via the relation

$$\Delta \boldsymbol{f} = \boldsymbol{f}(\boldsymbol{x}, \boldsymbol{b}, \boldsymbol{b}') - \boldsymbol{F}(\boldsymbol{x}, \boldsymbol{b}) \tag{3}$$

where $\boldsymbol{b}'$ are all forward function parameters which are ignored in the construction of $\boldsymbol{F}$, and $\Delta \boldsymbol{f}$ is the error in the forward model relative to the real physics.

We would like to illustrate the four terms in Eq. (1) via examples for ground-based infrared solar absorption spectrometry. *i*) The first term in Eq. (1), i.e., the smoothing error, is due to the limited vertical resolution, which ranges in the case of solar FTIR from 1–2 km up to nearly no resolution at all, depending on the species of interest and altitude. This results in a retrieved profile that is smoothed in comparison to the true profile which may show significant fine structure on the sub-kilometer vertical scale in the real atmosphere. *ii*) Typical model parameter errors (second term in Eq. 1). In the case of solar FTIR, there would be errors in the spectroscopic data used both for the target species and interfering species. Another example would be a wrong solar zenith angle (e.g., due to an error in instrument time) used for the ray-tracing calculations of

ACPD
6, 13027–13073, 2006

EGU

the solar absorption path. Also one of the most important error contributions in case of solar FTIR belongs to this class, namely temperature errors. Errors as large as a few Kelvin do occasionally arise, e.g., from a mismatch in time and space between nearby radio sondes used and the FTIR measurements. *iii*) A typical forward model error (third term in Eq. 1) in case of solar FTIR is the generalized use of Voigt type line shapes for all species and all lines, although it is know that deviations do occur, e.g., for a variety of water vapor or methane absorption lines in the mid-infrared atmospheric spectrum. If such a non-Voigt line is present in the micro-windows used, either as the target or as an interfering species, this forward model error will have an impact on the retrieved target profile. Other forward model errors could, e.g., arise from inadequate forward modeling of the instrumental line shape or channeling, if these effects are present in the spectra and cannot be retrieved. *iv*) The last error term in Eq. (1) is due to the spectral measurement noise which is transfered to the retrieval. Note that statistical analysis using a measurement noise covariance matrix takes noise correlations between neighboring spectral data points (or channels) into account. Such spectral correlations are present in the case of solar FTIR if a zero filling of the interferograms is performed.

In the following section we will show that a new class of errors, in addition to the four classes of Eq. (1), arises if we define a generalized state vector including not only the target profile, but also all further retrieval parameters. The effect is a split up of the first term of Eq. (1) into the smoothing error plus additional terms, which we will call interference errors. The rest of this paper is dedicated to these interference errors and their relation to smoothing errors. The error terms 2–4 of Eq. (1) will not be discussed further.

ACPD
6, 13027–13073, 2006

3 Theoretical description of interference errors

3.1 Generalized state vector

We now re-define $\boldsymbol{x}$ to be a "generalized state vector" which takes into account all parameters to be retrieved, not only the atmospheric target profile, see Eq. (4). We will refer to the part of $\boldsymbol{x}$ describing the atmospheric target profile to be retrieved as $\boldsymbol{t}$ with length n. It contains, for example, average volume mixing ratios of the target species, e.g., carbon monoxide, on a set of n=100 layers with thickness 1 km, covering the vertical range between 0–100 km altitude. The remaining sub-vector of $\boldsymbol{x}$ represents all further parameters to be retrieved in addition to the target parameters. It comprises vectors $\boldsymbol{v}_1$, $\boldsymbol{v}_2$, ... with length n, describing the profiles of interfering species, i.e., species different from the target species which show spectral signatures within the micro-windows as well as additional vector-type quantities that may be retrieved, such as retrieved temperature profiles (which can also cause an interference effect). Furthermore, it consists of scalar-type retrieval parameters s_1, s_2, ..., denoted as "retrieved auxiliary scalar parameters" hereafter. These parameters are candidates for forward model parameters that are retrieved, however, because they are not known accurately enough, e.g., a frequency shift between the measured and simulated spectrum (which can be caused by a frequency calibration error, either in the spectrometric measurement or the spectroscopic line data used). Note that we introduce the additional class "retrieved auxiliary scalar parameters" since, according to the nomenclature of Rodgers

ACPD
6, 13027–13073, 2006

(1976), “forward model parameters” are just parameters that are not being retrieved

$$\boldsymbol{x} := \begin{pmatrix} \boldsymbol{t} \\ \boldsymbol{v}_1 \\ \boldsymbol{v}_2 \\ \vdots \\ s_1 \\ s_2 \\ \vdots \end{pmatrix} = \begin{pmatrix} t_1 \\ \vdots \\ t_n \\ v_{11} \\ \vdots \\ v_{1n} \\ v_{21} \\ \vdots \\ v_{2n} \\ \vdots \\ s_1 \\ s_2 \\ \vdots \end{pmatrix} \tag{4}$$

It should be pointed out that the precondition for our later quantification of interference errors is, that not only the target species but also the interfering species (and all other retrieved vector-type quantities, e.g., temperature profiles) are represented within the state vector as full profiles with a sufficient number of grid elements n. This number has to be chosen large enough so that the true profile variations can be modeled by the forward model properly. For practical reasons we have to use the same vertical grid for the target species and interfering species (with, e.g., $n = 30 \ldots 100$ layers). This requirement is not met by the common practice, of retrieving interfering species using only one simple profile scaling factor. The problem is that, in this case, there is only one scalar entry to the state vector $\boldsymbol{x}$ from this interfering species (namely the scaling parameter), and, in consequence, there is no interface to link the true atmospheric profile covariance of the interfering species into the error analysis.

ACPD
6, 13027–13073, 2006

In order to overcome this difficulty we have to formally carry out a full profile retrieval including the interfering species which are intended to be retrieved via simple column scaling, but use at the same time a Tikhonov–type retrieval constraint with a very high regularization strength (see Sect. 3.3 for details). This approach emulates the intended effect of a simple profile scaling retrieval of the interfering species, and, at the same time, there is a full profile (i.e., vector-type) entry of the interfering species into the state vector. This is the precondition to allow a mapping of the true profile covariance into the error analysis (Sect. 3.2). We want to repeat that this somewhat laborious approach is necessary for an adequate analysis of the interference errors, i.e., this requirement does not originate from the (column) retrieval of the interfering species itself. However, we will see later, that application of a less regularized (profile) retrieval for the interfering species makes it possible to significantly reduce the interference errors (Sect. 5.2)

3.2 Smoothing errors and interference errors

We re-arrange and simplify Eq. (1) to the following form

$$\hat{\boldsymbol{x}} - \boldsymbol{x}_a = \mathbf{A}(\boldsymbol{x} - \boldsymbol{x}_a) + \boldsymbol{\varepsilon}_x \quad , \tag{5}$$

where $\boldsymbol{\varepsilon}_x$ comprises the error terms 2-4 in Eq. (1), i.e., all errors in the measurement and the forward model (parameters). $\mathbf{A}$ is the averaging kernel matrix which can be calculated analytically from the following relation (Steck, 2002)

$$\mathbf{A} = (\mathbf{K}^T \boldsymbol{S}_\varepsilon^{-1} \mathbf{K} + \mathbf{R})^{-1} \mathbf{K}^T \boldsymbol{S}_\varepsilon^{-1} \mathbf{K} \quad , \tag{6}$$

where $\mathbf{K}$ is the Jacobian of $\mathbf{F}$ with respect to $\boldsymbol{x}$, $\mathbf{S}_\varepsilon$ is the error covariance of the measurement, and $\mathbf{R}$ is the regularization matrix (see Sect. 3.3 for details). Alternatively, $\mathbf{A}$ can be calculated numerically by the so-called perturbation method, which uses the retrieval response to delta-function perturbations of subsequent components of $\boldsymbol{x}$ to fill the columns of $\mathbf{A}$. The appropriate magnitude of the perturbation can easily be found as a trade off between instabilities arising from perturbations which are too small due

ACPD
6, 13027–13073, 2006

EGU

to rounding errors, and saturation effects arising from perturbations which are too large due to non-linearity in the response.

Note that in Rodgers (1990) $\boldsymbol{x}$ is only the vector of the target species, i.e., what we designated by $\boldsymbol{t}$ above. In this paper, however, we define $\boldsymbol{x}$ as the full state vector comprising vectors for the target species and vectors for all interfering species and additional vector-type quantities retrieved, as well as the retrieved auxiliary scalar parameters, see Eq. (4). In consequence, $\mathbf{A}$ denotes in our case a generalized averaging kernel matrix which includes in addition rows and columns describing the interference of the retrieval of the target profile with the retrieval of all further parameters: inserting Eq. (4) into Eq. (5) yields

$$\hat{\boldsymbol{x}} - \boldsymbol{x}_a = \begin{pmatrix} \hat{\boldsymbol{t}} - \boldsymbol{t}_a \\ \hat{\boldsymbol{v}}_1 - \boldsymbol{v}_{1a} \\ \hat{\boldsymbol{v}}_2 - \boldsymbol{v}_{2a} \\ \vdots \\ \hat{s}_1 - s_{1a} \\ \hat{s}_2 - s_{2a} \\ \vdots \end{pmatrix} = \begin{pmatrix} \mathbf{A}_{tt} & \mathbf{A}_{tv1} & \mathbf{A}_{tv2} & \cdots & \boldsymbol{a}_{ts1}^T & \boldsymbol{a}_{ts2}^T & \cdots \\ \mathbf{A}_{v1t} & \mathbf{A}_{v1v1} & \mathbf{A}_{v1v2} & \cdots & \boldsymbol{a}_{v1s1}^T & \boldsymbol{a}_{v1s2}^T & \ddots \\ \mathbf{A}_{v2t} & \mathbf{A}_{v2v1} & \mathbf{A}_{v2v2} & \cdots & \boldsymbol{a}_{v2s1}^T & \boldsymbol{a}_{v2s2}^T & \ddots \\ \vdots & \ddots & \ddots & \ddots & \ddots & \ddots & \ddots \\ \boldsymbol{a}_{s1t} & \boldsymbol{a}_{s1v1} & \boldsymbol{a}_{s1v2} & \ddots & a_{s1s1} & a_{s1s2} & \ddots \\ \boldsymbol{a}_{s2t} & \boldsymbol{a}_{s2v1} & \boldsymbol{a}_{s2v2} & \ddots & a_{s2s1} & a_{s2s2} & \ddots \\ \vdots & \ddots & \ddots & \ddots & \ddots & \ddots & \ddots \end{pmatrix} \begin{pmatrix} \boldsymbol{t} - \boldsymbol{t}_a \\ \boldsymbol{v}_1 - \boldsymbol{v}_{1a} \\ \boldsymbol{v}_2 - \boldsymbol{v}_{2a} \\ \vdots \\ s_1 - s_{1a} \\ s_2 - s_{2a} \\ \vdots \end{pmatrix} + \begin{pmatrix} \boldsymbol{\varepsilon}_t \\ \boldsymbol{\varepsilon}_{v1} \\ \boldsymbol{\varepsilon}_{v2} \\ \vdots \\ \varepsilon_{s1} \\ \varepsilon_{s2} \\ \vdots \end{pmatrix} . \quad (7)$$

Our generalized averaging kernel matrix $\mathbf{A}$ comprises sub-matrices $\mathbf{A}_{ij}$, (column) vectors $\boldsymbol{a}_{ij}$, row vectors $\boldsymbol{a}_{ji}^T$, as well as scalars a_{ji}. Note that $\mathbf{A}_{tt}$ is what is usually called the "averaging kernel matrix" describing the smoothing of the retrieved target profile (Rodgers, 1990). Furthermore, if the retrieved auxiliary scalar parameters s_1, s_2, ... describe true physical scalar-type quantities (i.e., they are not scalar approximations to a vector-type physical quantity), and they are not correlated, then the retrieval of these scalars can and should be performed without any regularization. In this case Eq. (7)

ACPD
6, 13027–13073, 2006

EGU

simplifies to

$$\hat{\boldsymbol{x}} - \boldsymbol{x}_a = \begin{pmatrix} \hat{\boldsymbol{t}} - \boldsymbol{t}_a \\ \hat{\boldsymbol{v}}_1 - \boldsymbol{v}_{1a} \\ \hat{\boldsymbol{v}}_2 - \boldsymbol{v}_{2a} \\ \vdots \\ \hat{s}_1 - s_{1a} \\ \hat{s}_2 - s_{2a} \\ \vdots \end{pmatrix} = \begin{pmatrix} \mathbf{A}_{tt} & \mathbf{A}_{tv1} & \mathbf{A}_{tv2} & \cdots & 0 & 0 & \cdots \\ \mathbf{A}_{v1t} & \mathbf{A}_{v1v1} & \mathbf{A}_{v1v2} & \cdots & 0 & 0 & \ddots \\ \mathbf{A}_{v2t} & \mathbf{A}_{v2v1} & \mathbf{A}_{v2v2} & \cdots & 0 & 0 & \ddots \\ \vdots & \ddots & \ddots & \ddots & \ddots & \ddots & \ddots \\ 0 & 0 & 0 & \ddots & 1 & 0 & \ddots \\ 0 & 0 & 0 & \ddots & 0 & 1 & \ddots \\ \vdots & \ddots & \ddots & \ddots & \ddots & \ddots & \ddots \end{pmatrix} \begin{pmatrix} \boldsymbol{t} - \boldsymbol{t}_a \\ \boldsymbol{v}_1 - \boldsymbol{v}_{1a} \\ \boldsymbol{v}_2 - \boldsymbol{v}_{2a} \\ \vdots \\ s_1 - s_{1a} \\ s_2 - s_{2a} \\ \vdots \end{pmatrix} + \begin{pmatrix} \boldsymbol{\varepsilon}_t \\ \boldsymbol{\varepsilon}_{v1} \\ \boldsymbol{\varepsilon}_{v2} \\ \vdots \\ \varepsilon_{s1} \\ \varepsilon_{s2} \\ \vdots \end{pmatrix} . \quad (8)$$

We then obtain the following relation between $\hat{\boldsymbol{t}}$, $\boldsymbol{t}_a$, and $\boldsymbol{t}$

$$\hat{\boldsymbol{t}} - \boldsymbol{t}_a = \mathbf{A}_{tt}(\boldsymbol{t} - \boldsymbol{t}_\alpha) + \mathbf{A}_{tv1}(\boldsymbol{v}_1 - \boldsymbol{v}_{1a}) + \mathbf{A}_{tv2}(\boldsymbol{v}_2 - \boldsymbol{v}_{2a}) + \ldots + \boldsymbol{\varepsilon}_t \quad , \quad (9)$$

which can be rearranged

$$\begin{aligned} \hat{\boldsymbol{t}} - \boldsymbol{t} = {} & (\mathbf{A}_{tt} - \mathbf{I})(\boldsymbol{t} - \boldsymbol{t}_\alpha) && \ldots \text{ smoothing error} \\ & + \mathbf{A}_{tv1}(\boldsymbol{v}_1 - \boldsymbol{v}_{1a}) + \mathbf{A}_{tv2}(\boldsymbol{v}_2 - \boldsymbol{v}_{2a}) + \ldots && \ldots \text{ interference error} \\ & + \boldsymbol{\varepsilon}_t \end{aligned} \quad (10)$$

The first term is what has been defined by Rodgers (1990) as the "smoothing error" since it describes the differences between the retrieved profile $\hat{\boldsymbol{t}}$ and the true profile $\boldsymbol{t}$; these differences are due to the finite vertical resolution of the remote sounding system, or, in other words, due the fact that $\mathbf{A}_{tt}$ of real remote sounders deviates from the ideal unit matrix $\mathbf{I}$. The further terms are what we will refer to hereafter as "interference errors". They are caused by interference between the retrieval of the target profile $\boldsymbol{t}$ and the retrieval of the interfering species (and retrieved auxiliary quantities, e.g., temperature) with profiles $\boldsymbol{v}_1$, $\boldsymbol{v}_2$, ... We will call $\mathbf{A}_{tv1}$, $\mathbf{A}_{tv2}$, ... "interference kernel matrices".

The statistics of the smoothing error is described by the error covariance

$$\mathbf{S}_{tt} = (\boldsymbol{A}_{tt} - \mathbf{I})\, \mathbf{S}_t\, (\mathbf{A}_{tt} - \mathbf{I})^T , \quad (11)$$

ACPD
6, 13027–13073, 2006

EGU

where $\mathbf{S}_t$ is a best estimate of the true a priori covariance of the target profiles $\boldsymbol{t}$.

The statistics of the interference errors are described by the error covariance matrices

$$\begin{aligned} \mathbf{S}_{tv1} &= \mathbf{A}_{tv1}\,\mathbf{S}_{v1}\,\mathbf{A}_{tv1}^T \\ \mathbf{S}_{tv2} &= \mathbf{A}_{tv2}\,\mathbf{S}_{v2}\,\mathbf{A}_{tv2}^T \\ &\vdots \end{aligned} \quad , \tag{12}$$

where $\mathbf{S}_{v1}$, $\mathbf{S}_{v2}$, ... are best estimates of the true a priori covariances of the profiles $\boldsymbol{v}_1$, $\boldsymbol{v}_2$, ... of the interfering species (and retrieved auxiliary profile-type quantities, e.g., temperature).

3.3 Retrieval and different types of constraint

While the forward model maps from the n-dimensional state space (profiles, and further retrieval parameters) into the m-dimensional measurement space (spectrum), we are interested in the inverse mapping. Since $m>n$ holds in many cases, the inverse problem is formally over-determined, and can be formulated as a least squares problem. Usually, due to the non-linearity of $\boldsymbol{F}$ a Newtonian iteration is applied, and a regularization term is used that allows one to add additional information about the solution and thereby avoid oscillating profiles (Steck, 2002)

$$\begin{aligned} \boldsymbol{x}_{i+1} = \boldsymbol{x}_i &+ (\mathbf{K}_i^T \mathbf{S}_\varepsilon^{-1} \mathbf{K}_i + \mathbf{R})^{-1} \\ &\times \left\{ \mathbf{K}_i^T \mathbf{S}_\varepsilon^{-1} \left[\boldsymbol{y} - \boldsymbol{F}(\boldsymbol{x}_i) \right] - \mathbf{R}(\boldsymbol{x}_i - \boldsymbol{x}_a) \right\} \end{aligned} \quad , \tag{13}$$

where the subscript i denotes the iteration index.

In the following we briefly present two different types of regularization which we will use simultaneously for our analysis of interference errors, i.e., optimal estimation (Rodgers, 1976) and Tikhonov regularization (Tikhonov, 1963). We will apply optimal estimation to the retrieval of the target profile $\boldsymbol{t}$ (i.e., only to part part of the full state

ACPD
6, 13027–13073, 2006

EGU

vector $\boldsymbol{x}$); for the simultaneous retrieval of the interfering species $\boldsymbol{v}_1$, $\boldsymbol{v}_2$, ... Tikhonov regularization will be used. The reason for this will be explained below.

In the case of optimal estimation, $\mathbf{R}$ is set up using the relation $\mathbf{R}=\mathbf{S}_R^{-1}$ where $\mathbf{S}_R$ is the a priori covariance matrix. In the ideal case $\mathbf{S}_R$ is a climatological covariance constructed from an ensemble of true profiles covering the full range of possible atmospheric states. The a priori profile should be the true climatological mean for optimal estimation otherwise a bias will be introduced to the retrievals.

In the case of Tikhonov regularization, $\mathbf{R}$ is set up using the relation $\mathbf{R}=\alpha\mathbf{L}^T\mathbf{L}$, where α is the strength of the constraint and $\mathbf{L}$ is the constraint operator. For example, in case of the discrete first derivative operator $\mathbf{L}_1$ (Steck, 2002)

$$\mathbf{L}_1 = \begin{pmatrix} -1 & 1 & 0 & \dots & 0 \\ 0 & -1 & 1 & \ddots & \vdots \\ \vdots & \ddots & \ddots & \ddots & 0 \\ 0 & \dots & 0 & -1 & 1 \end{pmatrix} \tag{14}$$

the retrieved profile is constrained so that the difference between the retrieved and the a priori profile approaches a constant profile for high values of α. Regularization via the $\mathbf{L}_1$ operator constrains the shape of the retrieved profile but not the absolute values which are determined by the measurement. For the a priori profile either the true climatological mean can be adopted, or, if this is not know, any reasonable profile shape. In absence of any knowledge, it might even make sense to use a zero-a-priori to achieve a smoothing constraint. While means to optimize the magnitude of α for various purposes have been given by Steck (2002) in detail, we will restrict our discussion to two limiting cases: The case $\alpha \to 0$ describes a retrieval, where no regularization is performed at all, and in consequence the retrieved profiles will frequently suffer from oscillations. The other limiting case, i.e., $\alpha \to \infty$ represents a profile scaling retrieval which is a fitting via an iterative scaling of the a priori profile with one factor that is the same for all altitudes, i.e., an infinitely hard constraint to the profile shape and a zero

ACPD
6, 13027–13073, 2006

EGU

constraint to the absolute value of the scaling factor. We will use this kind of setting for retrieval of columns of the interfering species during our error analysis in Sect. 4.5.

It has been shown by Steck and von Clarmann (2001) in general terms that the optimal estimation formalism can be used to emulate purely Tikhonov-type smoothing constraints. We will just add one example for this equivalence which is of some relevance for our later discussion of interference errors. As explained above, a simple profile scaling retrieval can be set up by a Tikhonov $\mathbf{L}_1$-type constraint with $\alpha \rightarrow \infty$. This can be emulated by an optimal estimation retrieval, where the diagonal elements (variances) of $\mathbf{S}_R$ are large numbers (relative to the true variances) and the inter-layer correlation length (described by the off-diagonal elements of $\mathbf{S}_R$) is set to a high value (relative to the altitude range of the profile, e.g., 100 km).

3.4 Treatment of non-linearity for quantification of smoothing errors and interference errors

To solve the inverse problem and to analyze smoothing and interference errors we use the following linearization of the forward model

$$\boldsymbol{y} = \boldsymbol{F}(\boldsymbol{x}_0, \boldsymbol{b}_0) + \left.\frac{\partial \boldsymbol{F}}{\partial \boldsymbol{x}}\right|_{\boldsymbol{x}_0, \boldsymbol{b}_0} (\boldsymbol{x} - \boldsymbol{x}_0) + \boldsymbol{\varepsilon}_{\boldsymbol{y}} = \mathbf{K}|_{\boldsymbol{x}_0, \boldsymbol{b}_0} (\boldsymbol{x} - \boldsymbol{x}_0) + \boldsymbol{\varepsilon}_{\boldsymbol{y}} \quad (15)$$

around a linearization point $\boldsymbol{x}_0, \boldsymbol{b}_0$.

In linear approximation, the error analysis could be performed via one linearization point of the forward model. This point should be chosen to be the mean values $\bar{\hat{\boldsymbol{x}}}$ and $\bar{\boldsymbol{b}}$ calculated from the ensemble of i retrieved states $\hat{\boldsymbol{x}}_i$ and the corresponding input forward model parameters $\boldsymbol{b}_i$ that have been used for each retrieval.

However, for error analysis, the forward model is often not sufficiently linear, i.e., it does not allow for an appropriate description of the errors of the full ensemble of all possible values of parameters $\boldsymbol{x}$ and $\boldsymbol{b}$ using one linearization. Typical examples of causes leading to such a situation are *i*) the high variability of atmospheric profiles and columns (e.g., water vapor, either retrieved as target species $\boldsymbol{t}$ or as interfering species

ACPD
6, 13027–13073, 2006

EGU

v), and *ii*) the highly variable solar zenith angle which is a forward model parameter ***b*** in solar absorption spectrometry. In this case we will apply a statistical approach based on an ensemble of i linearizations with its linearization points ($\hat{\boldsymbol{x}}_i$,$\boldsymbol{b}_i$), i.e., the i retrieved states $\hat{\boldsymbol{x}}_i$ and the corresponding input forward model parameters $\boldsymbol{b}_i$ that have been used for each retrieval.

4 Quantification of interference errors of CO profiles from Zugspitze solar FTIR

4.1 Historical development of solar CO measurements

Although the first vertically resolved information on CO was obtained through in situ aircraft measurements in the 1970s (Seiler and Warneck, 1972; Seiler and Fishman 1981), ground-based remote sounding measurements were not made until a decade later. A set of Fourier Transform spectrometers for rotationally resolved solar absorption spectrometry in the mid-infrared spectral domain was set up in the early 1990s at a variety of stations around the globe within the framework of the NDACC network. In the beginning, only one spectral micro-window around the saturated R3 line of the fundamental (1-0) vibration-rotation absorption band was used for CO total column retrievals via profile scaling and non-linear least squares spectral fitting, and utilized, e.g., for satellite validation (Pougatchev et al., 1998). In the pioneering work by Pougatchev and Rinsland (1995) altitude information on CO was obtained for the first time from four different spectral micro-windows (simultaneously) including a set of 1-0 band lines with a variety of different opacities (i.e., R3, P7, P9, P10). This approach was varied and refined in a series of papers (Zhao et al., 1997; Rinsland et al., 1998). The most widely used approach is now the optimal estimation formalism of Rodgers (1976) semi-empirically modified for microwave profiling of stratospheric ozone (Connor et al., 1995) and applied to infrared CO retrievals using a reduced set of lines (R3, P7, P10) by Rinsland et al. (2000). A detailed error analysis of the Rinsland et al. (2000) CO retrieval (with slightly wider micro-windows) according to the Rodgers (1990) formal-

ism was presented by Rodgers and Connor (2003). We will refer to this maturated CO profile retrieval according to Rinsland et al. (2000) and Rodgers and Connor (2003) in the following as "RRC". A variety of applications of the RRC retrieval have been reported, e.g., for investigating the impact of biomass burning on the global CO distribution (Jones et al., 2001; Yurganov et al., 2004, 2005; Velazco et al., 2005; Paton-Walsh et al., 2005), as well as for satellite validation (Rodgers and Connor, 2003; Sussmann and Buchwitz, 2005).

4.2 Zugspitze FTIR CO measurement characteristics

At the NDACC Primary Station Zugspitze (47.42° N, 10.98° E, 2964 m a.s.l.), Germany, a Bruker 120 HR solar FTIR instrument was set up at the beginning of 1995 (Sussmann and Schäfer, 1997). Since then it has been operated continuously all year round with typically 120 measurement days per year, and is part of the Permanent Ground-Truthing Facility Zugspitze/Garmisch (Sussmann and Buchwitz, 2005; Sussmann et al., 2005a, b).

4.2.1 Test ensemble of Zugspitze spectra

Typical Zugspitze infrared spectra used for the CO profile retrievals are the average of 6 scans recorded in 14 min with an optical path difference of 250 cm^{-1}. Three spectral micro-windows from the 1-0 band were analyzed, i.e., 2057.785–2057.91 cm^{-1}, 2069.615–2069.71 cm^{-1}, and 2157.33–2159.15 cm^{-1}. For this paper we randomly selected a test ensemble of i=156 spectra taken after 1994. The average signal-to-rms-noise ratio of the spectra of this ensemble is 377:1. A significant problem in the forward model between 2157.77–2157.92 cm^{-1} was found in the final residuals of the spectral fits (measured minus calculated). The next section explains the reason for this.

ACPD
6, 13027–13073, 2006

EGU

4.2.2 Contribution plot and forward model characteristics

Figure 1 shows a contribution plot of the micro-windows used, i.e., a forward model simulation with the absorption contributions of the different species plotted separately. This contribution plot is based on the average SZA and the average of the retrieved states $\hat{\boldsymbol{x}}_i$ of our test ensemble. Note that there are four terrestrial interfering species, i.e., O_3 and CO_2 in the first two micro-windows and O_3, H_2O, N_2O, and CO_2 in the third micro-window. Furthermore, it can be seen that the residual problem found between 2157.77–2157.92 cm^{-1} (as mentioned in Sect. 4.2.1) is due to a solar CO line that has not been adequately modeled.

For the forward simulations we used the HITRAN 2000 spectroscopic line parameter compilation including the 2002 update (Rothmann et al., 2003). The model profiles are based on 66 layers with a 1 km width up to an altitude of 69 km altitude and 1 additional layer above (up to 100 km). For the pressure-temperature profile information used in the forward model we utilized the daily Munich radio sonde launched at 12:00 universal time about 80 km north of the Zugspitze.

4.3 Zugspitze FTIR CO retrieval settings

We use the SFIT2 (ver. 3.90) software and follow the RRC retrieval approach as described by Rinsland et al. (2000) and Rodgers and Connor (2003), with the modifications that follow.

4.3.1 CO a priori profile and full covariance for mid latitudes

To extend the RRC approach, we used a full CO a priori covariance matrix for the Zugspitze retrievals. This matrix was constructed from an ensemble of measured high resolution profiles. Earlier RRC had used a simple empirical a priori coaviance matrix for CO comprising diagonal elements only, with the standard deviations (stdv) for all layers either varied smoothly from 40% below 30 km to 20% above 40 km (Rinsland et

ACPD
6, 13027–13073, 2006

al., 2000), or all set to 100% (Rodgers and Connor, 2003). While these RRC retrieval settings were an empirical approach to stabilize the retrieval without too much influence from a priori information, the Zugspitze approach, for the first time, employs a strict application of the optimal estimation concept to the retrieval of CO profiles from solar FTIR.

The Zugspitze a priori profile $\boldsymbol{t}_a$ and a priori covariance matrix $\mathbf{S}_t = \mathbf{S}_{CO}$ for optimal estimation of CO was constructed from an ensemble of globally distributed aircraft CO measurements supplemented at above aircraft altitudes by a set of model output profiles used for the operational MOPITT retrieval (Deeter et al., 2003). In order to construct this prior information for the Zugspitze (47° N) mid latitude site we selected a subset of the Deeter et al. (2003) global profile set comprising all profiles within a full 47° N±16° latitudinal band (Fig. 2a). Figure 2a also shows the mean profile of this ensemble which is used as an a priori profile $\boldsymbol{t}_a$. The resulting a priori covariance matrix $\mathbf{S}_t = \mathbf{S}_{CO}$ was calculated from the statistics of the ensemble (Fig. 2b).

4.3.2 Error covariance S_ε and de-weighting

The measurement error covariance matrix $\mathbf{S}_\varepsilon$ was assumed to be diagonal. For the uncertainties of all spectral channels the average signal-to-noise ratio of the Zugspitze test ensemble was used (377:1). However, by inspecting the spectra in the interval between 2157.77–2157.92 cm^{-1} we were able to identify a systematic error in the solar CO forward simulation as the dominant source of error (Sects. 4.2.1 and 4.2.2). To prevent this error from being mapped into the retrieval, we performed a total de-weighting of the spectrum around this solar line by assuming a signal-to-noise ratio of 0:1 for this spectral domain within the $\mathbf{S}_\varepsilon$ matrix.

4.3.3 Retrieval of interfering species

A number of terrestrial interfering species with significant absorptions were found (O_3 and CO_2 in the first two micro-windows and O_3, H_2O, N_2O, and CO_2 in the third micro-

ACPD
6, 13027–13073, 2006

EGU

window) in the contribution plot of Fig. 1. We first retrieved them via column scaling retrieval. In spite of this, we had to introduce a full set of n-dimensional profile vectors $\boldsymbol{v}_1$, $\boldsymbol{v}_2$, ... for each of the interfering species (see Eq. 1), in order to attain a profile-type entry into the state vector. This is required for later analysis of the interference errors in the CO profiles which result from the true profile variability of the interfering species. In order to retrieve these interfering species we then used a Tikhonov $\mathbf{L}_1$-type constraint operator (see Eq. 14) with the regularization strength α initially set to a very high number (10^{13}), leading to a profile scaling retrieval (hard profile shape constraint) without any regularization/damping of the retrieved scaling factors. This setting leads to a degree of freedom of signal of dofs $\equiv 1$ per interfering species. Note, that we later find that the interference errors can be minimized by finding a lower optimum value for the regularization strength α for each interfering species, i.e., by actually performing profile retrievals for the interfering species (discussion in Sect. 5.2).

4.3.4 Retrieval of auxiliary parameters

For the Zugspitze CO profiling, the following auxiliary scalar parameters were retrieved. There is one independent frequency shift per micro-window, or a total of 3 parameters for all three micro-windows. One parameter is needed to fit possible zero line distortions via the saturated R3 line. Three more parameters are used to fit the background slope in each micro-window. There is also one auxiliary parameter to fit a frequency shift for the solar CO spectrum.

4.3.5 Retrieved test ensemble

Figure 3 shows the retrieved CO profiles from an arbitrarily chosen test ensemble of 156 Zugspitze spectra. It can be seen that the overall range of scatter of the retrieved ensemble is consistent with the ensemble of the aircraft profiles (also shown) from which our prior information (covariance and mean profile) was constructed.

ACPD
6, 13027–13073, 2006

4.4 Quantification of CO smoothing error

Averaging kernels of our CO profile retrieval (*i.e.*, the rows of $\mathbf{A}_{tt} = \mathbf{A}_{CO-CO}$, see Eq. 7) are plotted in Fig. 4. The plotted averaging kernels are averages of the averaging kernels calculated around all the retrieved states of the Zugspitze test ensemble (Fig. 3), i.e., they describe the mean retrieved state. The kernels peak close to their nominal altitude and retain close to unit area up to an altitude of 15 kilometers. The degree of freedom of signal is dofs = 3.3 on average over our test ensemble.

We calculate the smoothing error covariance $\mathbf{S}_{tt} = \mathbf{S}_{CO-CO}$ according to Eq. (11) using the a priori covariance $\mathbf{S}_t = \mathbf{S}_{CO}$ of Fig. 2b. Figure 5 shows the square roots of the diagonal elements of $\mathbf{S}_{CO-CO}$, i.e., error standard deviations as profiles versus altitude. Note that this is not a complete description of the smoothing errors, because they are correlated between different heights. However, it does provide an indication of the retrieval precision. Figure 5 shows the full ensemble of smoothing error profiles calculated around each retrieved state ($\hat{\boldsymbol{x}}_i$,$\boldsymbol{b}_i$) of the Zugspitze test ensemble. As described in Sect. 3.4 the reason for the spread of the smoothing errors is the non-linearity of the forward model and thus the dependency of the averaging kernels on the state ($\boldsymbol{x}_i$, $\boldsymbol{b}_i$).

Figure 5 also shows the natural CO variability as a function of altitude which has been calculated as the square root of the diagonal elements of the a priori covariance $\mathbf{S}_t = \mathbf{S}_{CO}$ (Fig. 2b). It can be seen that the magnitude of the smoothing error relative to the natural CO variability increases with altitude. However, the smoothing error of our retrieval never reaches or exceeds the magnitude of the natural CO variability, as expected for a properly set optimal estimation approach.

4.5 Quantification of interference errors

The statistics of the interference errors from the four interfering species, i.e., the interference error covariances $\mathbf{S}_{CO-O3}$, $\mathbf{S}_{CO-H2O}$, $\mathbf{S}_{CO-N2O}$, and $\mathbf{S}_{CO-CO2}$ are calculated thereafter according to Eq. (12). As an input to this we first have to calculate the interference kernel matrices $\mathbf{A}_{CO-O3}$, $\mathbf{A}_{CO-H2O}$, $\mathbf{A}_{CO-N2O}$, and $\mathbf{A}_{CO-CO2}$ (Sect. 4.5.1).

ACPD
6, 13027–13073, 2006

The second input to Eq. (12) are the a priori covariances for the interfering species $\mathbf{S}_{v1}$ =$\mathbf{S}_{O3}$, $\mathbf{S}_{v2}$ =$\mathbf{S}_{H2O}$, $\mathbf{S}_{v3}$ =$\mathbf{S}_{N2O}$, and $\mathbf{S}_{v4}$ =$\mathbf{S}_{CO2}$, which are presented in Sect. 4.5.2. Then Sect. 4.5.3 shows the resulting interference errors versus altitude and their comparison to the smoothing errors as well as to the natural variability of CO.

4.5.1 Interference kernels

The interference kernel matrices for our four interfering species are the quadratic submatrices $\mathbf{A}_{CO-O3,}\mathbf{A}_{CO-H2O,}\mathbf{A}_{CO-N2O}$, and $\mathbf{A}_{CO-CO2}$ of the generalized averaging kernel matrix as defined via Eq.(7). Analogously with the term "averaging kernels" we hereafter use the term "interference kernels" for the rows of these interference kernels matrices. They reflect the response of the CO-profile retrieval to a unit perturbation of the true profile of the interfering species (in arbitrary units of our state vector quantity, i.e., scaling factors of VMR-layer averages). The interference kernels for the four interfering species are plotted in Figs. 6a–d.

4.5.2 A priori covariances of the interfering species

To construct the a priori covariance $\mathbf{S}_{v1}$=$\mathbf{S}_{O3}$ needed to estimate the CO-O_3 interference error we used an ensemble of 1438 ozone sonde (brewer mast) profiles provided by the meteorological observatory Hohenpeissenberg. This German weather service site is located 30 km north of the Zugspitze. The Hohenpeissenberg ozone soundings are performed 3 times a week (i.e., Monday, Wednesday, and Friday), and our ensemble covers the time span January 1995–February 2006. Figure 7a shows the profile ensemble and its mean, and Fig. 7b shows the covariance calculated from this ensemble.

To construct the a priori covariance $\mathbf{S}_{v2}$=$\mathbf{S}_{H2O}$ we utilized the data set of the (4 times daily) radio soundings performed during the Garmisch AIRS validation campaign between 19 August–17 November 2002. Garmisch is located only 6 km from the Zugspitze horizontally. We used a subset of 66 radio sondes that had been launched

ACPD
6, 13027–13073, 2006

EGU

coincident to the solar FTIR measurements (i.e., filtering for clear sky conditions). This ensemble of water vapor profiles and the resulting covariance is plotted in Fig. 8.

To estimate the a priori covariance $\mathbf{S}_{v3} = \mathbf{S}_{N2O}$ we used an ensemble of 14 aircraft profiles from a number of campaigns performed from 1995 - 1997 between 20–70° N which were provided by the ETHmeg data base (http://www.megdb.ethz.ch/dbaccess.php), see Fig. 9.

The a priori covariance $\mathbf{S}_{v4}=\mathbf{S}_{CO2}$ was constructed from 134 profiles measured during two aircraft campaigns in July/August 2000 and May/June 2003 between 31–56° N. This data was provided by the ETHmeg data base, see Fig. 10.

4.5.3 Interference errors compared to the smoothing error

Based on the results of Sects. 4.5.1 and 4.5.2 the interference error covariances $\mathbf{S}_{CO-O3}$, $\mathbf{S}_{CO-H2O}$, $\mathbf{S}_{CO-N2O}$, and $\mathbf{S}_{CO-CO2}$ can be calculated according to Eq. (12). In analogy to Fig. 5 (illustrating the smoothing error versus altitude) we plot the square roots of the diagonal elements of the interference error covariances as profiles versus altitude, see Fig. 11a. Again, as for the smoothing error, we plotted the full ensemble of interference errors versus altitude calculated around each of the retrieved states of the Zugspitze test ensemble. The spread of the interference error profiles of one species is again due to non-linearity effects as discussed in Sect. 3.4 in general and in Sect. 4.4 for the case of smoothing errors. Figure 11a shows via an example a crucial result of this paper, namely, that interference errors can become comparable to the magnitude of the smoothing error or even larger: the CO-O_3 interference errors exceed the CO smoothing errors in the altitude range between ≈14–19 km and the CO-H_2O interference errors are comparable to the CO smoothing errors in the lower troposphere.

ACPD
6, 13027–13073, 2006

EGU

5 Sensitivity studies and minimization of interference errors

5.1 Experiment with widened micro-window

In the RRC micro-window set there is only one extremely weak water vapor feature at 2156.57 cm^{-1}, which is nearly hidden below the strong wing of the saturated CO R3 absorption line (Fig. 1c). Therefore, we decided to investigate the effect of widening this micro-window to the range 2156.0–2159.15 cm^{-1}, in order to include one additional, strong water line located at 2158.11 cm^{-1} (see grey shaded area in Fig. 1c). The question is, whether the CO-H_2O interference error is decreased or increased by widening the micro-window.

The answer can be seen by comparing Fig. 11b (based on the widened micro-window) with Fig. 11a (based on the RRC micro-window). Clearly, the CO-H_2O interference error is significantly larger when the micro-window is widened since the water vapor (profile scaling) retrieval is then dominated by the stronger 2156.57 cm^{-1} water line. Obviously, the HITRAN 2000 line strengths of the strong 2156.57 cm^{-1} water vapor line and the weaker 2158.11 cm^{-1} water vapor line are not perfectly consistent, leading to an increased residual around the weaker 2158.11 cm^{-1} water vapor line for retrieval from the wider micro window. And this increased water vapor residual is in the wing of the CO R3 line (where the weighting function yields information on CO) leading to an increased CO-H_2O interference error.

5.2 Optimizing the regularization strength of the retrieval of the interfering species

In this section we show that the interference errors can be reduced by changing the regularization of the retrieval of the interfering species from a simple scaling retrieval to a less regularized (profile) retrieval. The idea behind this is that a (less regularized) profile retrieval for an interfering species should lead to a smaller residual around the spectral feature of this interfering species (than scaling), and thus to less interference on the target species retrieval. The disadvantage is that a non-regularized profile

ACPD
6, 13027–13073, 2006

retrieval of an interfering species, in principle, leads to an effective "deweigthing" of the spectral domain where the interfering species absorbs, i.e., a reduced information content for the target species from this spectral domain, and thereby an increased smoothing error is expected. The trade-off between the two effects is illustrated hereafter.

Figure 12 shows on the horizontal scale the transition from a scaling retrieval (using the $\mathbf{L}_1$ operator in combination with very high values for the regularization parameter, *i.e.*, $\alpha_{O3} = 10^{13}$) towards an essentially non-regularized profile retrieval ($\alpha_{O3} = 10^{-11}$). The vertical scale in Fig. 12 shows "mean smoothing errors" (red curves) and "mean interference errors" (black curves). We define these as the altitude average (arithmetic mean up to 25 km) of the stdv-smoothing error profiles and stdv-interference error profiles plotted in Fig. 11, i.e.,

$$\begin{aligned} \bar{\sigma}_{CO-CO} &:= \sqrt{\sum_{i=1}^{n} \left(\mathbf{S}_{CO-CO}\right)_{ii} / n} \quad , \quad \ldots \text{ mean CO smoothing error} \\ \bar{\sigma}_{CO-O3} &:= \sqrt{\sum_{i=1}^{n} \left(\mathbf{S}_{CO-O3}\right)_{ii} / n} \quad , \quad \ldots \text{ mean CO – } O_3 \text{ interference error} \\ &\ldots \end{aligned} \tag{16}$$

These errors are calculated around all retrieved states of the Zugspitze test ensemble. The ensemble–type nature of these plots again results from the described non-linearity effects. As a result from Fig. 12 it can be seen, that the so-defined mean CO-O_3 interference error decreases for decreasing α_{O3} as expected. Figure 12 also shows that the mean CO smoothing error increases slightly with decreasing α_{O3}, which is also expected as outlined at the beginning of this section. Therefore, an optimum α_{O3} for the retrieval of the interfering species O_3 can be found by searching for the minimum of the combined error, i.e., $sqrt(\bar{\sigma}^2_{CO-CO}(\alpha_{O3}) + \bar{\sigma}^2_{CO-O3}(\alpha_{O3}))$, see green curves in Fig. 12. The resulting optimum setting for α_{O3} is found from the minimum of the average of all green curves (blue diamonds in Fig. 12), i.e., $\alpha_{O3} = 10^2$. The

ACPD
6, 13027–13073, 2006

EGU

optimization for α_{H2O}, α_{N2O}, and α_{CO2} was performed in an analogous manner and the results are summarized in Table 1. In the case of CO_2, the high value of $\alpha_{CO2} = 10^{13}$ means, that no further optimization relative to a scaling retrieval of CO_2 could be achieved.

The effect of incorporating these four optimized α-values into the retrieval is shown in Fig. 11c. The interference errors are significantly reduced compared to the RRC standard retrieval where all interfering species were retrieved via scaling (Fig. 11a), and are now much smaller than the smoothing error for all altitude regions. The corresponding effect on the altitude-averaged mean errors is shown in Table 2. Three different retrieval scenarios are given. Scenario *i*) corresponds to the RRC standard retrieval (Fig. 11a), i.e., the mean errors are given for the case in which all interfering species are retrieved via scaling. Scenario *ii*) corresponds to Fig. 11c, i.e., using the optimum α-values for all four interfering species. This reduces the mean CO-O_3 interference error down to 0.57%, which can be compared to the initial value of 3.12 % obtained in Scenario *i*). At the same time the mean CO smoothing error only increases slightly from 5.21% to 5.26%. In addition, the mean CO-H_2O interference error is decreased from 0.72 % down to 0.03 %. There is no major improvement for the mean CO-N_2O and CO-CO_2 interferences. The overall improvement of the "mean total error" $\bar{\sigma}_{tot} := sqrt(\bar{\sigma}^2_{CO-CO} + \bar{\sigma}^2_{CO-O3} + \bar{\sigma}^2_{CO-H2O} + \bar{\sigma}^2_{CO-N2O} + \bar{\sigma}^2_{CO-CO2})$ is 13.55%. Finally, Scenario *iii*) uses the optimum α-values only for O_3 and H_2O, while a scaling retrieval is used for N_2O and CO_2. The corresponding numbers in Table 2 show that the overall improvement is the same as for Scenario *ii*). Therefore, for a practical retrieval, Scenario *ii*) is to be preferred, since it requires less computational effort. We want to make the point that with both Scenarios *i*) and *ii*) the interference errors have been almost eliminated, since $\bar{\sigma}_{tot}$=5.29% of these Scenarios is only marginally (1.5%) higher than the smoothing error $\bar{\sigma}_{CO-CO}$= 5.21% of the standard Scenario *i*.

Finally we want add one remark about retrieval noise errors, forward model errors, and forward model parameter errors (see Eq. 1) which we have intentionally not treated in our examples. One might wonder whether errors belonging to these three classes

ACPD
6, 13027–13073, 2006

might increase or decrease due to our optimization of the α's of the interfering species. The answer is that in principle they will always decrease, i.e., our minimization of interference errors is always accompanied also by a reduction of retrieval noise errors and forward model (parameter) errors. This can be seen from analogy to the finding by Steck (2000, see Fig. 4 therein): as a result of a change in (target species) regularization strength (to higher or lower values, respectively) the smoothing error is shifted, in principle, in the same direction (higher or lower values, respectively) and both retrieval noise errors and forward model (parameter) errors are shifted in the opposite direction. This finding for a varied target species regularization can directly be transferred to our case of changing interfering species regularization since the latter is directly linked to changes of the effective target species regularization: As mentioned above, any increase or decrease in the regularization strength of the interfering species has the effect of weighting the target species retrieval to a higher or lower degree in the spectral range where the interfering species absorbs.

6 Summary and conclusions

This paper shows that a class of potentially significant errors exists in infrared remote sounding of profiles of atmospheric composition that has not been treated in the literature up to now. This new class of "interference errors" supplements the well-know traditional classes of "smoothing errors," "forward model errors," "forward model parameter errors," and "retrieval noise errors," formulated this way in classical error analysis of optimal estimation by Rodgers. Interference errors are a concern for atmospheric spectroscopy in the infrared domain, since many vibration-rotation bands of different trace species overlap there. This is not the case in the microwave atmospheric spectrum. Optimal estimation was first applied to microwave sounders, and this might be a historical reason, why classical error analysis did not include the treatment of interference errors. The interference effect physically originates from spectral residuals due to any type of regularization of the retrieval of interfering species which then lead to

ACPD
6, 13027–13073, 2006

artifacts in target species retrieval.

A general theoretical formulation of interference errors is given. It is based on a generalized state vector comprising all retrieval parameters, including the interfering species in addition to the target species. The point is made, that even in the usual case of an intended retrieval of interfering species via simple profile scaling, a full profile (i.e., vector-type) entry has to be introduced into the state vector. We show how this can be achieved for the interfering species by formally implementing a profile retrieval using the Tikhonov-type first order regularization matrix (with a very high regularization strength), which effectively emulates a scaling retrieval. This leads then to a generalized averaging kernel matrix comprising the classical averaging kernels plus the newly-defined interference kernels. The latter are used for estimating the interference error, using realistic climatological covariances describing the true atmospheric variability of the interfering species.

The general formulation is illustrated by applying it to a real sounding situation. This is demonstrated for the example of optimal estimation of CO profiles from ground-based solar infrared spectra recorded with the high-resolution Fourier Transform spectrometer at the NDACC Primary Station Zugspitze, Germany. The errors resulting to the CO profiles from CO-O_3, CO-H_2O, CO-N_2O, and CO-CO_2 interferences are quantified in detail. A crucial result of this paper is that interference errors can become comparable to the magnitude of the smoothing error or even larger: For the widely used standard CO retrieval approach the CO-O_3 interference errors exceed the CO smoothing errors in the altitude range between ≈14–19 km, and CO-H_2O interference errors are comparable to the CO smoothing errors in the lower troposphere.

Part of our general theoretical formulation is that in principle effects from non-linearity of the retrieval effect the magnitude of the interference errors (and smoothing errors). This is because interference kernels (and averaging kernels) depend in principle on the true state at the time of measurement within the range of possible atmospheric states encountered and the range of possible forward model parameters (e.g., varying actual solar zenith angles). In consequence, the smoothing errors and interference

ACPD
6, 13027–13073, 2006

EGU

errors show a state dependency. This principle effect is shown to play a significant role in a real sounding situation. This is illustrated by the example of CO standard profile retrievals from solar FTIR, which show that interference errors and smoothing are in fact varying by a factor of two and more, depending on the state. This implies that the common practice in the infrared community of using just one "typical" averaging kernel for characterization of a retrieval does not hold in general and has to be reconsidered on a case-to-case basis. Therefore, throughout the example section of this paper smoothing errors and interference errors are computed around an ensemble of states retrieved from a test ensemble of Zugspitze solar FTIR spectra.

We present two case studies showing how the error analysis can be utilized for reducing interference errors, e.g., via changed micro-window sets or optimized regularization constraints for the retrieval of the interfering species. The first case study, again for the example of solar FTIR CO retrievals, shows that a widened micro-window including one additional (stronger) water line leads to strongly increased interference errors. This is due to inconsistencies in the water vapor line strengths in the HITRAN data base. In the second case study it is shown that a profile retrieval for the interfering species (instead of a simple profile scaling) can significantly reduce the interference errors. A scheme to systematically minimize the interference errors is suggested. This scheme is based on a Tikhonov–type retrieval for the interfering species using the first-derivative regularization operator and optimizing the regularization parameter. In this case it is shown (for the example of optimal estimation of CO profiles from solar FTIR spectra) that the interference errors become negligible by using Tikhonov-type profile retrievals for the interfering species O_3 and H_2O with regularization parameters $\alpha_{O3}= 10^2$, $\alpha_{H2O}= 10^0$.

Interference errors have not been treated in a rigorous and quantitative way up to now, although, a theoretical formulation for the treatment of all further classes of possible errors (i.e., smoothing errors, forward model parameter errors, forward model errors, and errors from measurement noise) have previously been described in the literature. Therefore, we have not discussed these further classes of possible errors in

ACPD
6, 13027–13073, 2006

EGU

the example section of this paper. However, we conjectured that simultaneous optimization of smoothing and interference errors would also lead to lower retrieval noise and forward model (parameter) errors.

This paper shows how to identify and quantify interference errors, and how to minimize the total error including interference errors and the smoothing error. The general formulation is illustrated for the example of solar FTIR spectrometry of CO profiles. However, the findings of this paper can be applied to soundings of all infrared-active atmospheric trace gases, which are more than two dozen gases with relevance to climate and ozone. Morereover, these findings hold for all kind of infrared remote sounding systems, i.e., retrievals from ground-based, balloon-borne, airborne, or satellite spectroradiometers.

Acknowledgements. We thank W. Seiler (IMK-IFU) for his continuous interest in this work, and W. Stremme (IMK-IFU) for valuable scientific discussions. It is a pleasure to acknowledge encouraging discussions with B. Connor (NIWA) as to the basic approach pursued in this paper to quantify interference errors. We would also like to thank H. Claude (German Weather Service) for providing the Hohenpeissenberg ozone sonde data and D. Brunner (EMPA) for making available aircraft profiles via access to the ETHmeg data. Basic funding of the NDACC Primary Station Zugspitze/Garmisch and Permanent Ground-Truthing Facility Zugspitze/Garmisch has been provided by the German Federal Ministry of Education and Research (BMBF) via the Program "Atmosphere and Climate" of the German Helmholtz Association of National Research Centres. Funding by the EC within the projects UFTIR (contract EVK2-CT-2002-00159) and HYMN (contract GOCE 037048) is gratefully acknowledged. This work contributes to the ESA-ENVISAT-Validation-Project TASTE and is part of the EC-Network of Excellence ACCENT-TROPOSAT-2.

References

Connor, B. J., Parrish, A., Tsou, J.-J., and McCormick, M. P.: Error analysis for the ground-based microwave ozone measurements during STOIC, J. Geophys. Res., 100, 9283–9291, 1995.

Deeter, M. N., Emmons, L. K., Francis, G. L., Edwards, D. P., Gille, J. C., Warner, J. X., Khattatov, B., Ziskin, D., Lamarque, J.-F., Ho, S.-P., Yuding, V., Attie, J.-L. Packman, D., Chen, J., Mao, D., and Drummond, J. R.: Operational carbon monoxide retrieval algorithm and selected results for the MOPITT instrument, J. Geophys. Res., 108, 4399–4409, 2003.

Jones, N. B., Rinsland, C. P., Liley, J. B., and Rosen, J.: Correlation of aerosol and carbon monoxide at 45° S: Evidence of biomass burning emissions, Geophys. Res. Lett., 28, 709–712, 2001.

Paton-Walsh, C., Jones, N. B., Wilson, S. R., Haverd, V., Meier, A., Griffith, D. W. T., and Rinsland, C. P.: Measurements of trace gas emissions from Australian forest fires and correlations with coincident measurements of aerosol optical depth, J. Geophys. Res., 110, D24305, doi:10.1029/2005JD006202, 2005.

Pougatchev, N. S. and Rinsland, C. P.: Spectroscopic study of the seasonal variation of carbon monoxide vertical distribution above Kitt Peak, J. Geophys. Res., 100, 1409–1416, 1995.

Pougatchev, N. S., Jones, N. B., Connor, B. J., Rinsland, C. P., Becker, E., Coffey, M. T., Connors, V.S., Demoulin, P., Dzhola, A.V., Fast, H., Grechko, E.I., Hannigan, J. W., Koike, M., Kondo, Y., Mahieu, E., Mankin, W.G., Mittermeier, R. L., Notholt, J., Reichle Jr, H. G., Sen, B., Steele, L.P., Toon, G. C., Yurganov, L. N., Zander, R., and Zhao, Y.: Ground-based infrared solar spectroscopic measurements of carbon monoxide during 1994 Measurement of Air Pollution from Space flights, J. Geophys. Res., 103(D15), 19 317–19 325, 1998.

Rinsland, C. P., Jones, N. B., Connor, B. J., Logan, J. A., Pougatchev, N. S., Goldman, A., Murcray, F. J., Stephen, T. M., Pine, A. S., Zander, R., Mahieu, E., and Demoulin, P.: Northern and southern hemisphere ground-based infrared spectroscopic measurements of tropospheric carbon monoxide and ethane, J. Geophys. Res., 103, 28 197–28 217, 1998.

Rinsland, C. P., Mahieu, E., Zander, R., Demoulin, P., Forrer, J., and Buchmann, B.: Free tropospheric CO, C_2H_6, and HCN over central Europe: Recent measurements from the Jungfraujoch station including the detection of elevated columns during 1998, J. Geophys. Res., 105, 24 235–24 249, 2000.

Rodgers, C. D.: Retrieval of Atmospheric Temperature and Composition From Remote Measurements of Thermal Radiation, Rev. Geophys. Space Phys., 14, 609–624, 1976.

Rodgers, C. D.: Characterization and Error Analysis of Profiles Retrieved From Remote Sounding Measurements, J. Geophys. Res., 95, 5587–5595, 1990.

Rodgers, C. D.: Inverse Methods for Atmospheric Sounding: Theory and Practice, vol. 2 of Series on Atmospheric, Oceanic and Planetary Physics, edited by: Taylor, F. W., World

Scientific, 2000.
Rodgers, C. D. and Connor, B. J.: Intercomparison of remote sounding instruments, J. Geophys. Res., 108(D3), 4116, doi:10.1029/2002JD002299, 2003.
Rothmann, L. S., Barbe, A., Benner, D. C., Brown, L. R., Camy-Peyret, C., Carleer, M. R., Chance, K., Clerbaux, C., Dana, V., Devi, V. M., Fayt, A., Flaud, J. M., Gamache, R. R., Goldman, A., Jacquemart, D., Jucks, K. W., Lafferty, W. J., Mandin, J. Y., Massie, S. T., Nemtchinov, V., Newnham, D. A., Perrin, A., Rinsland, C. P., Schroeder, J., Smith, K. M., Smith, M. A. H., Tang, K., Toth, R. A., Vander Auwera, J., Varanasi, P., and Yoshino, K.: The HITRAN molecular spectroscopic database: edition of 2000 including updates through 2001, J. Quant. Spectrosc. Radiat. Transfer, 82, 5–44, 2003.
Seiler, W. and Warneck, P.: Decrease of carbon monoxide mixing ratio at the tropopause, J. Geophys. Res., 77, 3204–3214, 1972.
Seiler, W. and Fishman, J., The distribution of carbon monoxide and ozone in the free troposphere, J. Geophys. Res., 86, 7255–7265, 1981.
Steck, T. and von Clarmann, T.: Constrained profile retrieval applied to the observation mode of the Michelson Interferometer for Passive Atmospheric Sounding, Appl. Opt., 40, 3559–3571, 2001.
Steck, T.: Methods for determining regularization for atmospheric retrieval problems, Appl. Opt., 41, 1788–1797, 2002.
Sussmann, R. and Schäfer, K.: Infrared spectroscopy of tropospheric trace gases: combined analysis of horizontal and vertical column abundances, Appl. Opt., 36, 735–741, 1997.
Sussmann, R. and Buchwitz, M.: Initial validation of ENVISAT/SCIAMACHY columnar CO by FTIR profile retrievals at the Ground-Truthing Station Zugspitze, Atmos. Chem. Phys., 5, 1497–1503, 2005, http://www.atmos-chem-phys.net/5/1497/2005/.
Sussmann, R., Stremme, W. Buchwitz, M., and de Beek, R.: Validation of ENVISAT/SCIAMACHY columnar methane by solar FTIR spectrometry at the Ground-Truthing Station Zugspitze, Atmos. Chem. Phys., 5, 2419–2429, 2005a.
Sussmann, R., Stremme, W., Burrows, J.P., Richter, A., Seiler, W., and Rettinger, M.: Stratospheric and tropospheric NO_2 variability on the diurnal and annual scale: a combined retrieval from ENVISAT/SCIAMACHY and solar FTIR at the Permanent Ground-Truthing Facility Zugspitze/Garmisch, Atmos. Chem. Phys., 5, 2657–2677, 2005b,
Tikhonov, A.: On the solution of incorrectly stated problems and a method of regularization,

Dokl. Acad. Nauk SSSR, 151, 501–504, 1963.
Velazco, V., Notholt, J., Warneke, T., Lawrence, M., Bremer, H., Drummond, J., Schulz, A., Krieg, J., and Schrems, O.: Latitude and altitude variability of carbon monoxide in the Atlantic detected from ship-borne Fourier transform spectrometry, model, and satellite data, J. Geophys. Res., 110, D09306, doi:10.1029/2004JD005351, 2005.
Yurganov, L. N., Blumenstock, T., Grechko, E. I., Hase, F., Hyer, E. J., Kasischke, E. S., Koike, M., Kondo, Y., Kramer, I., Leung, F.-Y., Mahieu, E., Mellqvist, J., Notholt, J., Novelli, P. C., Rinsland, C. P., Scheel, H. E., Schulz, A., Strandberg, A., Sussmann, R., Tanimoto, H., Velazco, V., Zander, R., and Zhao, Y.: A quantitative assessment of the 1998 carbon monoxide emission anomaly in the Northern Hemisphere based on total column and surface concentration measurements, J. Geophys. Res., 109, D15305, doi:10.1029/2004JD004559, 2004.
Yurganov, L. N., Duchatelet, P., Dzhola, A. V., Edwards, D. P., Hase, F., Kramer, I., Mahieu, E., Mellqvist, J., Notholt, J., Novelli. P. C., Rockmann, A., Scheel, H. E., Schneider, M., Schulz, A., Strandberg, A., Sussmann, R., Tanimoto, H., Velazco, V., Drummond, J. R., and Gille, J. C.: Increased Northern Hemispheric carbon monoxide burden in the troposphere in 2002 and 2003 detected from the ground and from space, Atmos. Chem. Phys., 5, 563–573, 2005,
Zhao, Y., Kondo, Y., Murcray, F.J., Liu, X., Koike, M., Kita, K., Nakajima, H., Murata, I., and Suzuki, K.: Carbon monoxide column abundances and tropospheric concentrations retrieved from high resolution ground-based infrared solar spectra at 43.5 ° N over Japan, J. Geophys. Res., 102(D19), 23 403–23 411, 1997.

Table 1. Optimum settings of the regularization strength α for retrieval of the interfering species O_3, H_2O, N_2O, and CO_2 found from linear minimization of interference and smoothing errors.

α_{O3}	α_{H2O}	α_{N2O}	α_{CO2}
10^2	10^0	10^5	10^{13}

ACPD
6, 13027–13073, 2006

EGU

Table 2. Results of the combined minimization of interference errors and smoothing errors; "opt. α" refers to the numbers given in Table 1.

mean errors / α-settings	$\overline{\sigma}_{CO-CO}$	$\overline{\sigma}_{CO-O3}$	$\overline{\sigma}_{CO-H2O}$	$\overline{\sigma}_{CO-N2O}$	$\overline{\sigma}_{CO-CO2}$	$\overline{\sigma}_{tot}$	improvement versus scaling
Scenario i) scaling for all interfering species	5.21 %	3.12 %	0.72 %	0.09 %	0.01 %	6.12 %	
Scenario ii) opt. α used for all interf. species	5.26 %	0.57 %	0.03 %	0.04 %	0.01 %	5.29 %	13.55 %
Scenario iii) opt. α used for O_3 and H_2O, scaling for N_2O and CO_2	5.26 %	0.57 %	0.03 %	0.08 %	0.01 %	5.29 %	13.55 %

ACPD
6, 13027–13073, 2006

EGU

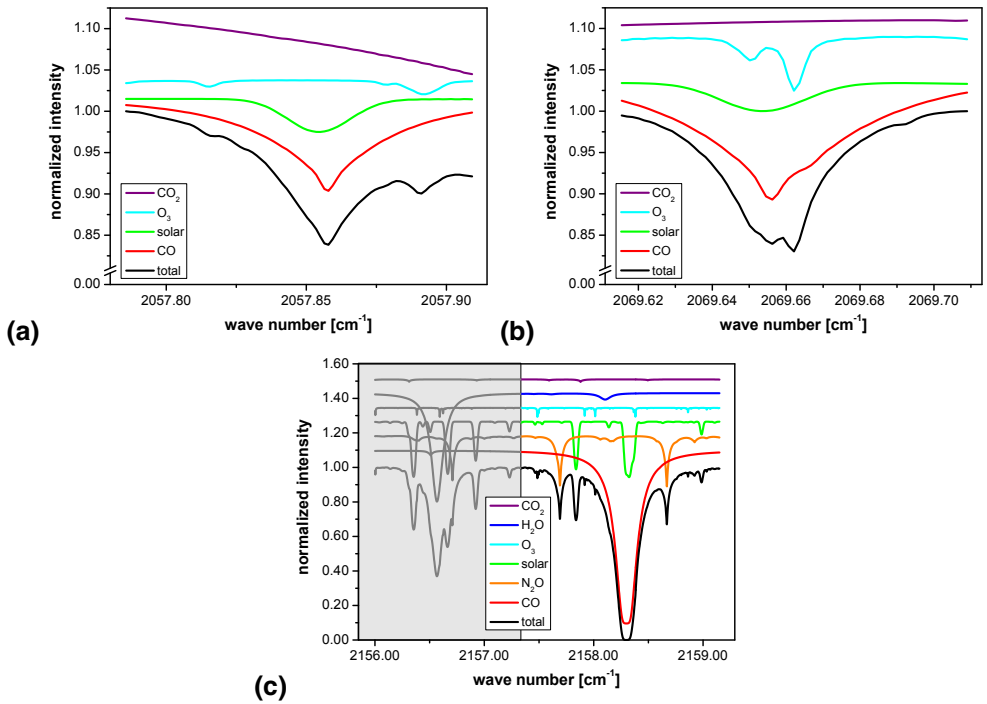

Fig. 1. Forward calculation of the three micro-windows **(a)**–**(c)** of the solar infrared absorption spectrum used for CO profile retrievals. The contributions of the different absorbing species are separated. Note, that the grey-shaded spectral area in (c) is not used for the standard retrieval. It is only used for the sensitivity study with the widened micro-window in Sect. 5.1.

ACPD
6, 13027–13073, 2006

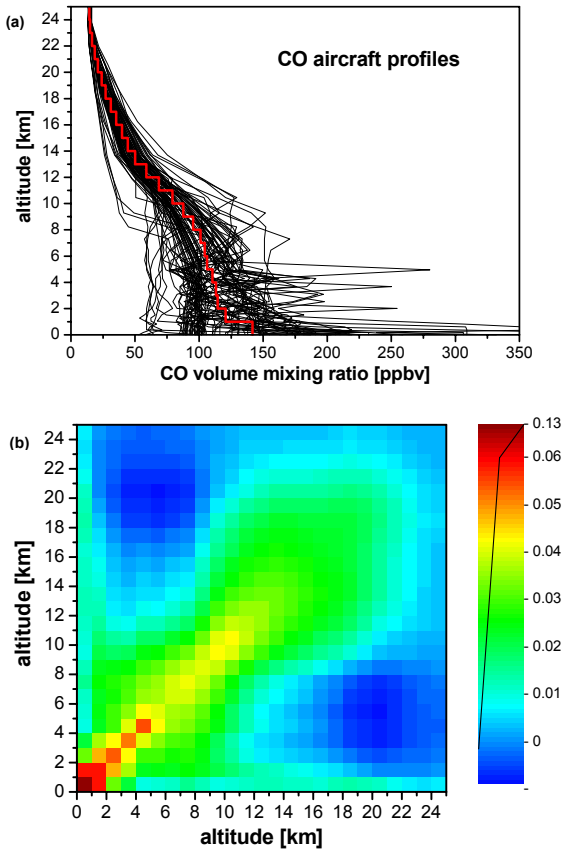

Fig. 2. Climatological ensemble of CO aircraft profiles used to construct the Zugspitze CO a priori profile **(a)** and the CO a priori covariance **(b)**. Note, that the state vector quantity for the CO profile retrieval is scaling factors of the a priori VMR profile given in a 1-km layer grid.

ACPD
6, 13027–13073, 2006

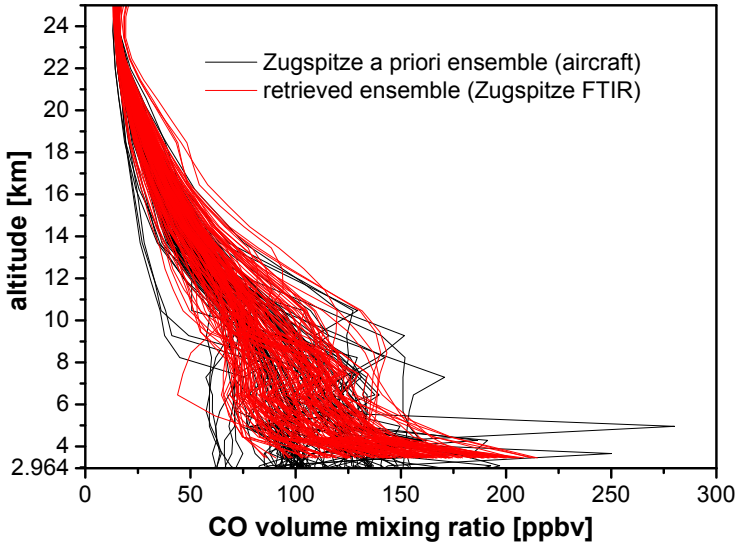

Fig. 3. CO profiles retrieved via optimal estimation from a test ensemble of 156 Zugspitze solar FTIR spectra plotted together with the climatological aircraft profile ensemble used to construct the a priori information (see also Fig. 2).

ACPD
6, 13027–13073, 2006

EGU

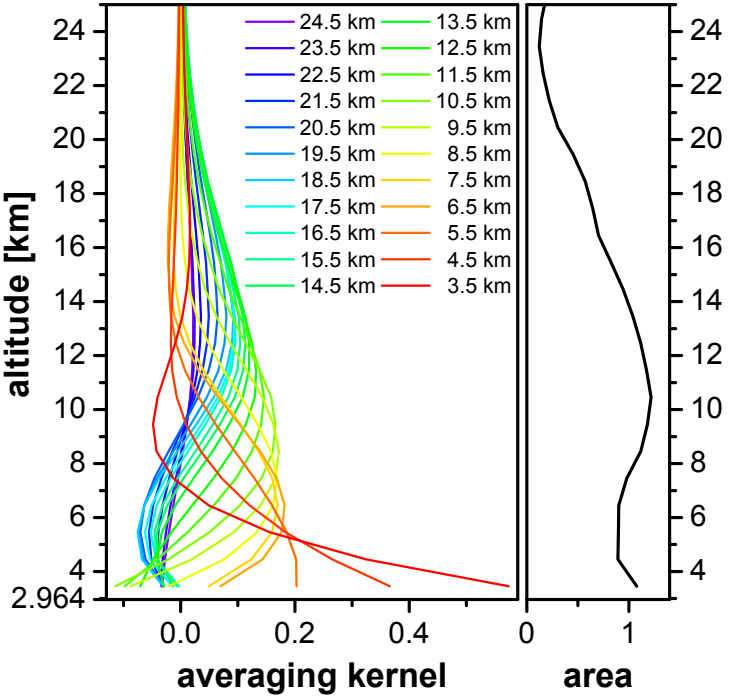

Fig. 4. Averaging kernels (rows of the averaging kernel matrix) for the Zugspitze standard retrieval of CO profiles via optimal estimation. The nominal altitudes of the kernels are given as well as the areas of the kernels as a function of altitude (black curve in the right part). Note, that the averaging kernels are calculated for the state vector quantity for the CO retrieval, which is scaling factors of the a priori VMR profile given in a 1-km layer grid. The kernels plotted are the average of the kernels calculated around all states retrieved from the Zugspitze test ensemble of 156 spectra.

ACPD
6, 13027–13073, 2006

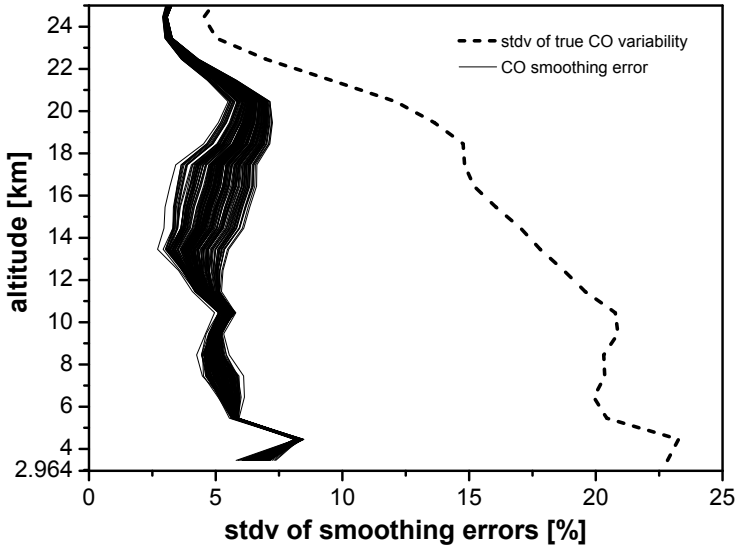

Fig. 5. Profile of the stdv of the true CO variability (dashed line: square roots of the diagonal elements of the climatological CO covariance) and ensemble of smoothing error profiles (solid lines: square roots of the diagonal elements of the smoothing error covariance) calculated around all states retrieved from the Zugspitze test ensemble of 156 spectra. The ensemble type nature of the smoothing errors is a result of the non-linearity of the retrieval (i.e., the averaging kernels) with respect to the different possible states.

ACPD
6, 13027–13073, 2006

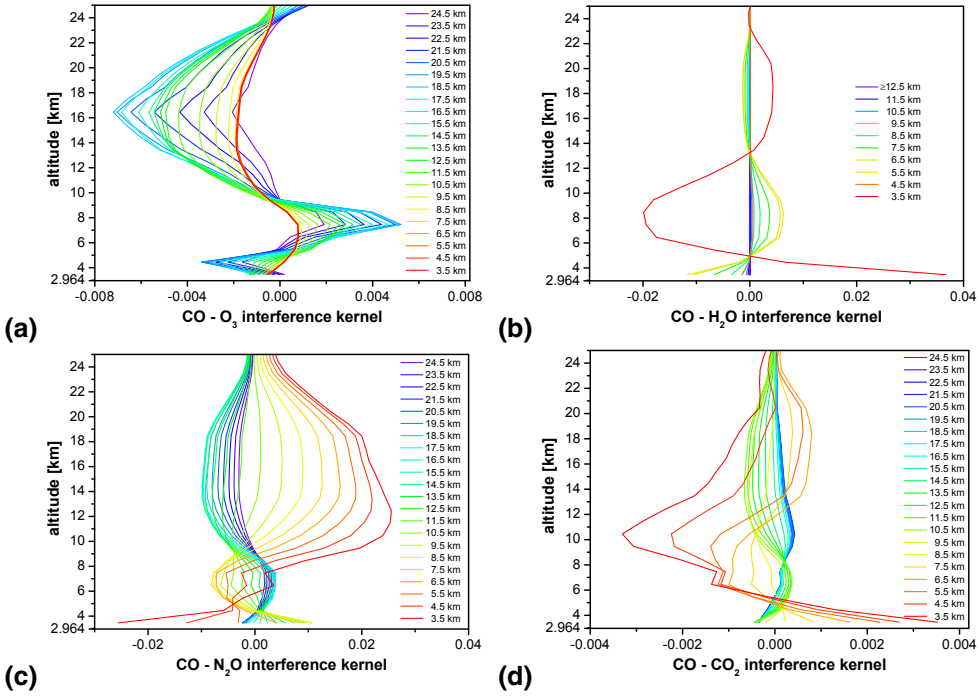

Fig. 6. Interference kernels (rows of the interference kernel matrices) for the interfering species O_3 **(a)**, H_2O **(b)**, N_2O **(c)**, and CO_2 **(d)** impacting the standard retrieval of CO profiles. The nominal altitude of the kernels is given. Note, that the kernels are calculated for the state vector quantity for the retrieval, which is scaling factors of the a priori VMR profiles given in a 1-km layer grid. The interference kernels plotted are the average of the kernels calculated around all states retrieved from the Zugspitze test ensemble of 156 spectra.

ACPD
6, 13027–13073, 2006

EGU

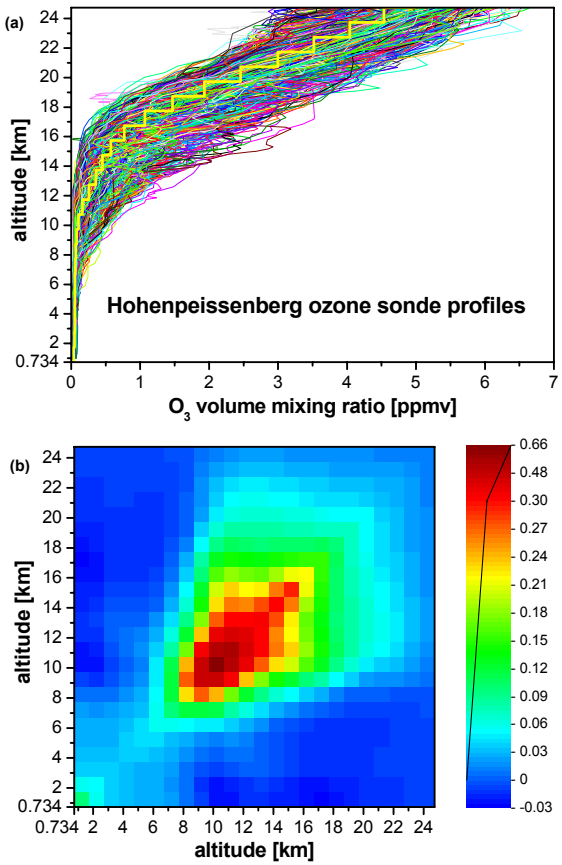

Fig. 7. Climatological ensemble of ozone sonde profiles used to construct the Zugspitze O_3 a priori profile **(a)** and the O_3 climatological covariance **(b)**. Note, that the state vector quantity for the retrieval is scaling factors of the a priori VMR profile given in a 1-km layer grid.

ACPD
6, 13027–13073, 2006

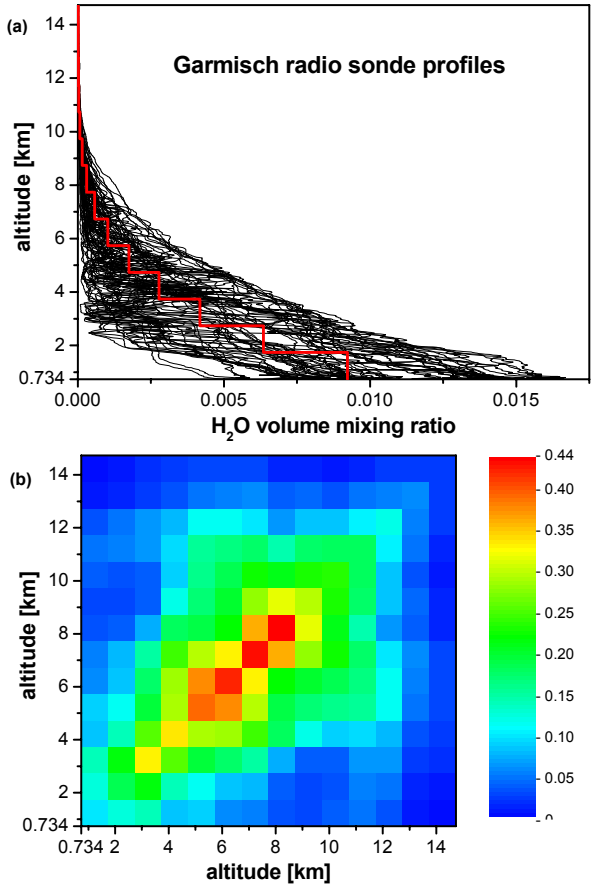

Fig. 8. Climatological ensemble of radio sonde profiles used to construct the Zugspitze H_2O a priori profile **(a)** and the H_2O climatological covariance **(b)**. Note, that the state vector quantity for the retrieval is scaling factors of the a priori VMR profile given in a 1-km layer grid.

ACPD
6, 13027–13073, 2006

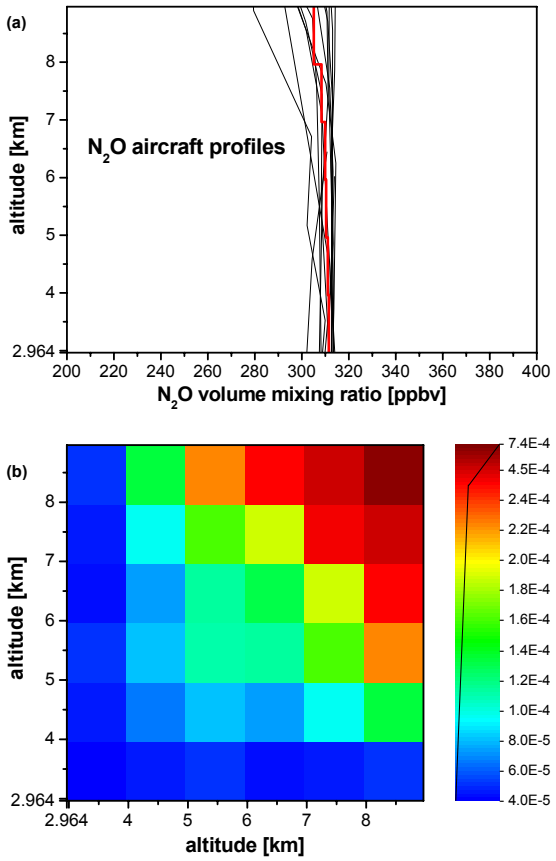

Fig. 9. Climatological ensemble of aircraft profiles used to construct the Zugspitze N_2O a priori profile **(a)** and the N_2O climatological covariance **(b)**. Note, that the state vector quantity for the retrieval is scaling factors of the a priori VMR profile given in a 1-km layer grid.

ACPD
6, 13027–13073, 2006

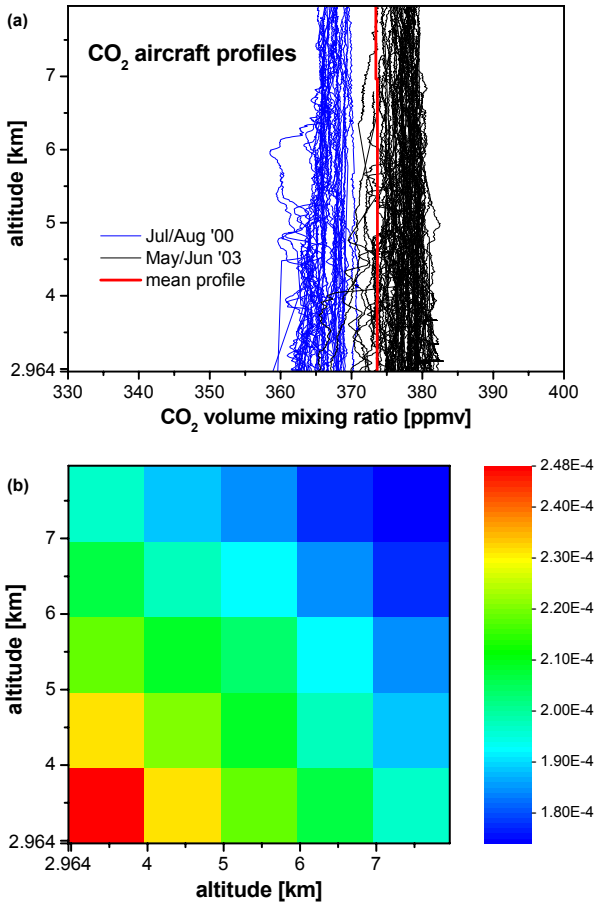

Fig. 10. Climatological ensemble of aircraft profiles used to construct the Zugspitze CO_2 a priori profile **(a)** and the CO_2 climatological covariance **(b)**. Note, that the state vector quantity for the retrieval is scaling factors of the a priori VMR profile given in a 1-km layer grid.

ACPD
6, 13027–13073, 2006

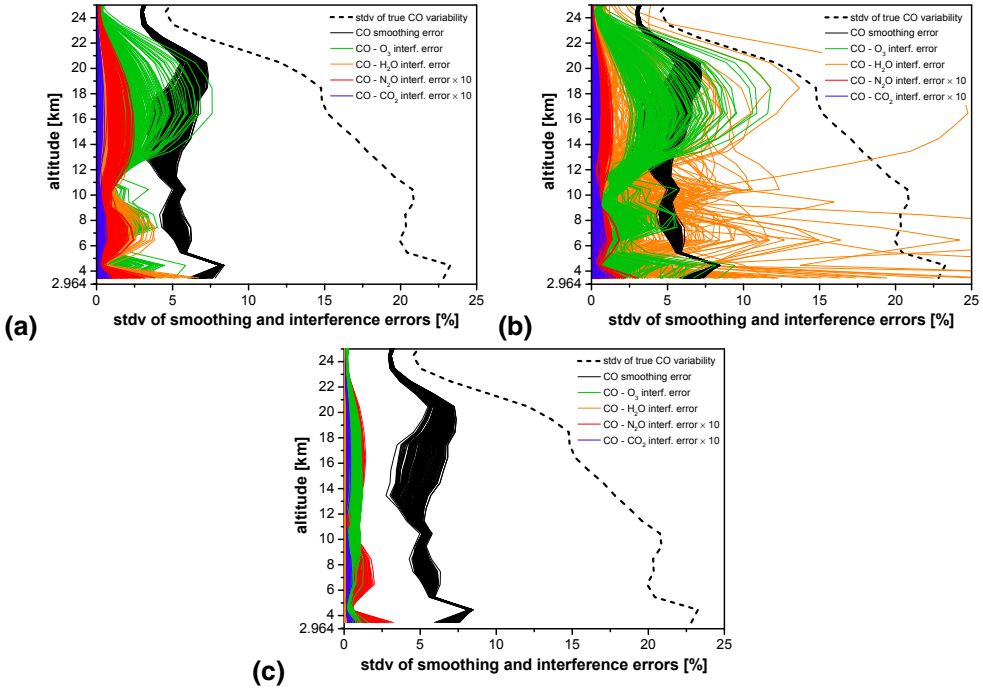

Fig. 11. **(a)** Analogous plot to Fig. 5. In addition, the profiles of the interference errors CO-O_3, CO-H_2O, CO-N_2O and CO-CO_2 are plotted (colored curves: square roots of the diagonal elements of the interference error covariances) which have been calculated around all states retrieved from the Zugspitze test ensemble of 156 spectra. The ensemble type nature of the interference errors is a result of the non-linearity of the retrieval (i.e., the interference kernels) with respect to the different possible states. **(b)** Same as (a) but for widened micro-window as indicated in Fig. 1c. **(c)** Same as (a) but for optimized (profile) retrievals for the interfering species using the regularization parameters given in Table 1.

ACPD
6, 13027–13073, 2006

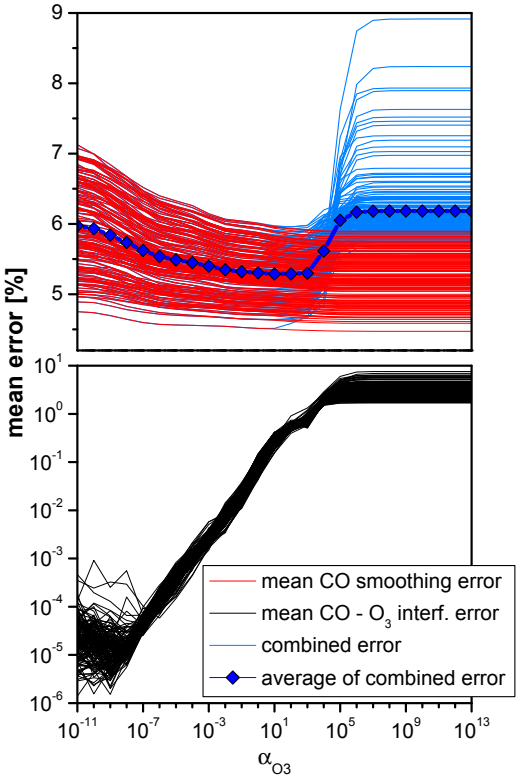

Fig. 12. This image displays the trade-off between minimizing interference errors and the smoothing error. Plotted are altitude averaged CO smoothing errors (red curves) and CO-O_3 interference errors (black curves) calculated around all states retrieved from the 156 spectra of the Zugspitze test ensemble as a function of the regularization strength α_{O3}. The ensemble type nature of the plots is due to non-linearity effects. The combined CO smoothing and CO-O_3 interference errors are plotted (blue curves), and their average (blue diamonds) shows a minimum for $\alpha_{O3}=10^2$.

ACPD
6, 13027–13073, 2006